Formation and desorption of sulphur chains (H_2S_x and S_x) in cometary ice effects of ice composition and temperature

Carrascosa, H.; Muñoz Caro, G. M.; Martín-DomCrossed D sign©nech, R.; Cazaux, S.; Chen, Y. J.; Fuente, A.

DOI
10.1093/mnras/stae1768

Publication date
2024

Document Version
Final published version

Published in
Monthly Notices of the Royal Astronomical Society

Monthly Notices of the ROYAL ASTRONOMICAL SOCIETY

MNRAS **533,** 967–978 (2024) https://doi.org/10.1093/mnras/stae1768
Advance Access publication 2024 July 22

Formation and desorption of sulphur chains (H_2S_x and S_x) in cometary ice: effects of ice composition and temperature

H. Carrascosa,[1]★ G. M. Muñoz Caro,[1]★ R. Martín-Doménech,[1]★ S. Cazaux,[2,3] Y.-J. Chen[4] and A. Fuente[1]

[1]*Centro de Astrobiología (CAB,CSIC–INTA), Ctra. de Ajalvir, km 4, Torrejón de Ardoz, E-28850 Madrid, Spain*
[2]*Faculty of Aerospace Engineering, Delft University of Technology, 2629, Delft, the Netherlands*
[3]*Leiden Observatory, Leiden University, PO Box 9513, NL-2300 RA Leiden, the Netherlands*
[4]*Department of Physics, National Central University, Jhongli City, Taoyuan County 32054, Taiwan*

Accepted 2024 July 17. Received 2024 July 17; in original form 2024 June 26

ABSTRACT

The reservoir of sulphur accounting for sulphur depletion in the gas of dense clouds and circumstellar regions is still unclear. One possibility is the formation of sulphur chains, which would be difficult to detect by spectroscopic techniques. This work explores the formation of sulphur chains experimentally, both in pure H_2S ice samples and in H_2O:H_2S ice mixtures. An ultrahigh vacuum chamber, ISAC, eqquipped with FTIR and QMS, was used for the experiments. Our results show that the formation of H_2S_x species is efficient, not only in pure H_2S ice samples, but also in water-rich ice samples. Large sulphur chains are formed more efficiently at low temperatures (≈10 K), while high temperatures (≈50 K) favour the formation of short sulphur chains. Mass spectra of H_2S_x, $x = 2$–6, species are presented for the first time. Their analysis suggests that H_2S_x species are favoured in comparison with S_x chains. Nevertheless, the detection of several S_x^+ fragments at high temperatures in H_2S:H_2O ice mixtures suggests the presence of S_8 in the irradiated ice samples, which could sublimate from 260 K. ROSINA instrument data from the cometary *Rosetta* mission detected mass-to-charge ratios 96 and 128. Comparing these detections with our experiments, we propose two alternatives: (1) H_2S_4 and H_2S_5 to be responsible of those S_3^+ and S_4^+ cations, respectively, or (2) S_8 species, sublimating and being fragmented in the mass spectrometer. If S_8 is the parent molecule, then S_5^+ and S_6^+ cations could be also detected in future missions by broadening the mass spectrometer range.

Key words: astrochemistry – methods: laboratory: molecular – techniques: spectroscopic – ISM: molecules – ultraviolet: ISM.

1 INTRODUCTION

Sulphur chemistry in molecular clouds and circumstellar regions is a key factor to address the sulphur depletion problem. The cosmic abundance of sulphur is well-reproduced in diffuse clouds (Jenkins 2009). However, the abundance of sulphur atoms in the species detected in dense interstellar clouds is orders of magnitude lower than cosmic abundance (Penzias et al. 1971; Oppenheimer & Dalgarno 1974; Bulut et al. 2021). Therefore, a reservoir of sulphur atoms should be present in these environments. Caselli, Hasegawa & Herbst (1994) hypothesized that S atoms could constitute a reservoir on the surface of dust grains. More recently, Laas & Caselli (2019) used the depletion mechanism proposed by Ruffle et al. (1999), including the formation of S-bearing organic species to reproduce the abundances of sulphur in the interstellar medium (ISM). They concluded that sulphur may be relatively abundant in organic species, as the calculated abundances agreed with observations. Nevertheless, the molecular mechanisms leading to sulphur depletion remain unclear.

The formation of polysulphides (H_2S_x) is important in the astrochemical context, related to the sulphur depletion problem. Furthermore, these molecules can play an important role in biological systems, as they are present in microorganisms, acting as reducing agents in different metabolic routes. The formation and subsequent incorporation of polysulphides into biological systems is not known (Kharma et al. 2019). If present in comets, these molecules were delivered to the early Earth, in particular during the Heavy Bombardment that ended 3.8 billion years ago.

Other studies by Jiménez-Escobar & Muñoz Caro (2011) proposed that sulphur atoms may be present in allotropic forms of sulphur, being supported theoretically by Shingledecker et al. (2020). Hereafter, we will refer to H_2S_x and S_x molecules as polysulphides and sulphur allotropes, respectively. Furthermore, the more general term 'sulphur chains' will be used to refer to both families of species indistinctly. Sulphur chains would be hard to detect by spectroscopic techniques. Cazaux et al. (2022) studied the formation of sulphur chains from pure H_2S ice samples submitted to radiation and warmup, both experimentally and using Monte Carlo simulations. They concluded that the formation of these species takes place in pure H_2S ice samples, and they may constitute a sulphur reservoir in the ISM.

A dust grain travelling from the diffuse medium to a molecular cloud will experiment decreasing temperatures. Radiation and

★ E-mails: hcarrascosa@cab.inta-csic.es (HC); munozcg@cab.inta-csic.es (GMMC); rmartin@cab.inta-csic.es (RMD)

temperature in the diffuse cloud break any covalent bonds that may be formed, avoiding the formation of molecules. Between the diffuse and the dense cloud, known as the translucent phase, sulphur atoms can accrete on the surface of dust grains, what could contribute to the observed sulphur depletion (Cazaux et al. 2022). Once in the dense region, the lower radiation allows the formation and survival of molecules. Hydrogenation of oxygen and sulphur atoms impinging the dust surface induce the formation of H_2O and H_2S molecules (Duley, Millar & Williams 1980). Above H_2S thermal desorption temperature (≈90 K under laboratory conditions, or ≈50 K in space; Collings et al. 2004) H_2S will not be retained in the ice mantle. Deeper in the cloud, temperature is lower, and both H_2O and H_2S will be adsorbed on the surface of dust grains, forming a mixed layer. However, if most of the H_2O has been incorporated to the ice mantle at higher temperatures, a H_2S-rich layer may be formed. Therefore, understanding sulphur chemistry in dense clouds requires the study of not only H_2S chemistry, but also H_2S chemistry in a H_2O matrix.

The *Rosetta* mission to comet 67P/Churyumov–Gerasimenko was devoted to understand the surface composition of comets, to shed light on their formation and evolution. The detection of sulphur species during the *Rosetta* mission by mass spectrometry was done using two techniques: (1) by an *in situ* spectrometer, COSAC (Cometary Sampling and Composition Experiment), onboard of the Philae lander, and (2) using ROSINA (Rosetta Spectrometer for Ion and Neutral Analysis), an orbiter spectrometer.COSAC detected molecules with a mass-to-charge ratio up to 60 (Goesmann et al. 2015), therefore avoiding detection of any species containing more than one sulphur atom. Indeed, no S-species were identified in their data. However, the extended measuring range of ROSINA (up to 140 mass-to-charge units) and the multiple measurements of the desorbing species made it possible to measure the presence of molecules containing more than one sulphur atom (Calmonte et al. 2016; Mahjoub et al. 2023).

Calmonte et al. (2016) reported the presence of mass-to-charge ratios of 96 and 128, which were attributed to S_3^+ and S_4^+ cations. However, these authors could not confirm the presence of S_3 and S_4 molecules, as their detections could be originated by larger sulphur species being fragmented into S_3^+ and S_4^+ fragments. Mass spectra data for these type of molecules are required to better constrain the parent species resulting in these detections. Recently, Mahjoub et al. (2023) used ROSINA data to analyse the presence of sulphur-bearing species in the coma of 67P. They reported the presence of H_2S_3 molecules (i.e. mass-to-charge ratio of $\frac{m}{z} = 98$). Therefore, the combined data from Calmonte et al. (2016) and Mahjoub et al. (2023) could imply the presence of H_2S_3 molecules which may be fragmented into S_3^+. Analogous processes could also be present involving larger H_2S_x species.

Cazaux et al. (2022) and Altwegg et al. (2022) made experiments on the formation of H_2S_x and S_x species containing up to four sulphur atoms. Apparently, there is no reason to constrain the chain length of sulphur chains in these experiments. However, the detection limits of the analytical techniques could not allow to determine whether large chains may be formed. Indeed, S_8, and other sulphur species in lower abundances, were reported in the residues made from similar experiments containing H_2S (Muñoz Caro 2002).

This work is focused in the understanding of the mechanisms leading to the formation and desorption of larger H_2S_x and S_x chains. The presence of these species may constitute a large sulphur reservoir which may help to decipher the sulphur depletion problem. Results are compared with works from Calmonte et al. (2016) and Mahjoub et al. (2023).

Thermal desorption temperatures for H_2S_x species are determined in this paper, and their mass spectra are provided for the first time (Section 3.1). Section 3.2 studies the effect induced by a water-matrix surrounding H_2S molecules. In particular, the capability of sulphur species to react together forming sulphur chains in these astrophysical scenarios will be shown. The effect of temperature in the photoprocessing of the ice samples is discussed for both H_2S pure and H_2S:H_2O ice mixtures in Section 3.3. Section 4 compares the experimental results obtained with reported data from *Rosetta* mission. Finally, conclusions and astrophysical implications are presented in Section 5.

2 EXPERIMENTAL

Experiments were carried out using the Interstellar Astrochemistry Chamber (ISAC) set-up, at Centro de Astrobiología (CAB, CSIC-INTA). ISAC is fully described in Muñoz Caro et al. (2010). Briefly, ISAC is an ultrahigh vacuum chamber designed to mimic the conditions in the ISM regarding pressure, temperature, and ultraviolet (UV) radiation. The base pressure in ISAC is in the 10^{-11} mbar range, obtained by the use of turbomolecular and getter pumps. The lowest temperature, 10 K, which is measured on top of the sample-holder, is reached using a closed-cycle He cryostat, connected to a silicon diode. This system allows a precise control of temperature between 10 and 300 K, with an accuracy better than 0.1 K. UV radiation is obtained using a microwave discharged hydrogen lamp (MDHL) from Opthos Instruments, and a controlled hydrogen flux with a pressure of 0.4 mbar. The MgF_2 window between the MDHL and the ice sample absorbs UV radiation for wavelengths shorter than 114 nm (Chen et al. 2014). For pure H_2S ice samples, H_2S (Nippon gases, 99.8 per cent) was used, and highly distilled MilliQ water obtained from a Millipore water distribution system IQ-7000 was used for H_2S:H_2O ice mixtures.

Gas-phase in ISAC is constantly monitored with a quadrupole mass spectrometry, using a Pfeiffer Prisma quadrupole equipped with a Channeltron detector. Molecules are ionized by electron impact at 70 eV. Solid phase is monitored after deposition and irradiation and during warm up of the ice samples with Fourier-transform infrared spectroscopy (FTIR), using a Bruker Vertex 70 spectrometer equipped with a deuterated triglycine sulphate detector (DTGS) in transmittance mode. For each measurement, 128 IR spectra were averaged with a resolution of 2 cm^{-1}.

Ice samples were deposited from the gas-phase through a stainless steel tube oriented towards the MgF_2 substrate (≈3 cm away). H_2S column density was fixed in the experiments, by growing the ice for 3 h at a constant pressure of 2×10^{-7} mbar, monitoring the ion current of $\frac{m}{z} = 34$ with a quadrupole mass spectrometer. Regarding H_2S:H_2O ice mixtures, H_2S was introduced at the same pressure, to ensure the same amount of H_2S molecules in the ice samples. H_2O was introduced through a different gas line, at the required pressure to obtain the 1:4 mixture desired, by monitoring $\frac{m}{z} = 18$. The high UV absorption of H_2S molecules (Cruz-Diaz et al. 2014), together with the large column density fixed for this work determined the impossibility of irradiating after deposition of the ice, as only the top ≈100 monolayers would absorb photon energy. Instead, simultaneous deposition and irradiation was used for the experiments. Temperature programmed desorption (TPD) experiments were also carried out at 1 K min^{-1}, devoted to detect the presence of so-formed photoproducts during their sublimation with the QMS.

Table 1 shows the different experiments carried out for this work. H_2O column density (N) was obtained from the IR spectrum after

Table 1. Experiments performed in this work. $\frac{m}{z} = 34$ column shows the normalized (with respect to the value in Exp. **1**) integrated area recorded by the QMS during deposition of the ice samples for H_2S molecules. These values were used to calculate the total H_2S column density deposited during each experiment (*initial column density*). $N(H_2S)$ and $N(H_2O)$ represent the column density measured after simultaneous deposition and irradiation of H_2S and H_2O, respectively. Last column shows H_2S destruction estimated from the calculation of the initial column density and the measured column density after photoprocessing of the ice samples.

Exp.	Ice sample	T (K)	Dep. time (min)	$\frac{m}{z} = 34$ (normalized)	Photon dose ($\times 10^{17}$ cm^{-2})	$N_f(H_2S)$ ($\times 10^{17}$ cm^{-2})	$N_f(H_2O)$ ($\times 10^{17}$cm^{-2})	H_2S destruction per cent
1	H_2S	10	180	1	0	15	0	0
2	H_2S	10	178	1.2	6.4	7.3	0	58
3	H_2S	50	182	1.1	6.1	8.3	0	48
4	H_2S: H_2O (1:4)	10	180	0.9	3.9	6.1	37	53
5	H_2S: H_2O (1:4)	50	186	0.8	5.0	3.8	46	67

simultaneous deposition and irradiation of ice samples using a band strength (A) of 1.9×10^{-16} cm molecule^{-1} at 10 K and 2.1×10^{-16} cm molecule^{-1} at 50 K (Mastrapa et al. 2009), and equation (1), where τ_v is the optical depth of the band, and dv the wavenumber differential. For H_2S, the available ice column density was obtained from the blank experiment using the IR spectrum and a band strength of 2.2×10^{-17} cm molecule^{-1} at 10 K (Cazaux et al. 2022), in agreement with the band strength provided by Yarnall & Hudson (2022). As the deposition time and H_2S partial pressure were kept constant for all the experiments, H_2S column density was assumed to be the same for all the experiments. This linear relationship between the column density of accreted ice and deposition time is presented in González Díaz et al. (2022), see fig. 8 of this paper.

$$N = \frac{1}{A} \int_{\text{band}} \tau_v \, \mathrm{d}v. \tag{1}$$

To calculate the H_2S destruction in the experiments, H_2S column density after deposition and irradiation was obtained from the IR spectrum, using a band strength of 2.2×10^{-17} cm^{-2} at 10 K and 2.0×10^{-17} cm^{-2} at 50 K (Cazaux et al. 2022), subtracting it from the available column density calculated from the blank experiment, and considering the signal measured by the QMS for $\frac{m}{z} = 34$, shown in Table 1.

3 RESULTS AND DISCUSSION

Generalizing the synthetic pathway towards the formation of relatively short polysulphides reported by Cazaux et al. (2022), the formation of H_2S_x species could take place in subsequent additions of HS· radicals produced from UV irradiation to any H_2S_x species:

$$H_2S + HS\cdot \rightarrow H_2S_2 + H\cdot \tag{2}$$

...

$$H_2S_x + HS\cdot \rightarrow H_2S_{x+1} + H\cdot \tag{3}$$

Hydrogen atoms produced from above reactions will diffuse in the ice, desorbing if they reach the surface, forming molecular H_2, or reforming H_2S molecules. However, it is also possible that radical–radical reactions take place:

$$HS\cdot + HS\cdot \rightarrow H_2S_2. \tag{4}$$

Not only HS· radicals are formed, but any other $HS_x\cdot$ radicals may be formed upon UV irradiation. Therefore, large H_2S_x chains could be formed following equations (5) or (6):

$$H_2S_x + HS_y\cdot \rightarrow H_2S_{x+y} + H\cdot \tag{5}$$

$$HS_x\cdot + HS_y\cdot \rightarrow H_2S_{x+y}. \tag{6}$$

Similar processes can be responsible of the formation of sulphur allotropes from sulphur atoms:

$$S\cdot + S\cdot \rightarrow S_2. \tag{7}$$

...

$$S_x\cdot + S_y\cdot \rightarrow S_{x+y}. \tag{8}$$

Sulphur allotropes can be also produced from dehydrogenation of sulphur chains, what may be specially favoured if a cyclic allotrope (number of sulphur atoms greater than five) is obtained:

$$H_2S_x \rightarrow H_2 + S_x. \tag{9}$$

3.1 Pure H_2S ice samples

Fig. 1 shows the QMS data obtained during thermal desorption of an irradiated pure H_2S ice sample (Exp. **2**). Each panel is related to thermal desorption of a given H_2S_x species, with x = 1–6. Thermal desorption of H_2S was detected at 88 K. $\frac{m}{z} = 64$ and $\frac{m}{z} = 66$ are also detected co-desorbing with H_2S, but blank experiments confirmed that the observed signals are mostly due to contamination of S_2 ($^{32}S_2$ and $^{32}S^{34}S$) and a small fraction of H_2S_2 during deposition of the ice sample. The recorded intensity for $\frac{m}{z} = 64$ and $\frac{m}{z} = 66$ during warming up of H_2S in Exp. **2** was attributed to the same contamination. Same behaviour was observed for H_2S ice samples deposited and irradiated at 50 K (Exp. **3**, data not shown).

Thermal desorption of H_2S_2, H_2S_3, and H_2S_4 (panels 2, 3, and 4 in Fig. 1) take place at 136, 172, and 194 K, in well agreement with those reported by Cazaux et al. (2022). Furthermore, the larger H_2S column density used in these experiments compared to Cazaux et al. (2022) allows to detect the presence of larger and less abundant H_2S_x species. Panel 3 in Fig. 1 shows thermal desorption of $\frac{m}{z} = 96$ at 194 K. It is related to S_3^+ cation. S_3^+ could be produced from direct ionization of S_3 molecules in the QMS. However, by looking at the mass spectra, it is clear that $\frac{m}{z} = 96$ is co-desorbing with $\frac{m}{z} = 130$, shown in panel 4, suggesting that S_3^+ is a fragment from the parent H_2S_4 molecule. The same behaviour was found for H_2S_5 ($\frac{m}{z} = 162$) and S_4^+ fragment ($\frac{m}{z} = 128$) at 219 K. Therefore, it is expected that larger species would show a similar fragmentation pattern, allowing the detection of H_2S_6 (241 K) and H_2S_7 (259 K) by the corresponding S_5^+ ($\frac{m}{z} = 160$) and S_6^+ ($\frac{m}{z} = 192$) fragments present in panels 6 and 7 in Fig. 1.

Fig. 2 shows the normalized intensity of the molecular ion, M^+, for H_2S_x, x = 1–6, and $\frac{m}{z} = 64$, measured at their thermal desorption maximum during TPD. The decrease in the M^+ is indicative of the fragmentation of the species in the QMS. On the other hand, the increase for $\frac{m}{z} = 64$ fragment, which becomes most prominent in the mass spectra for H_2S_x, $x \geq 3$, suggests that $\frac{m}{z} = 64$ fragment will

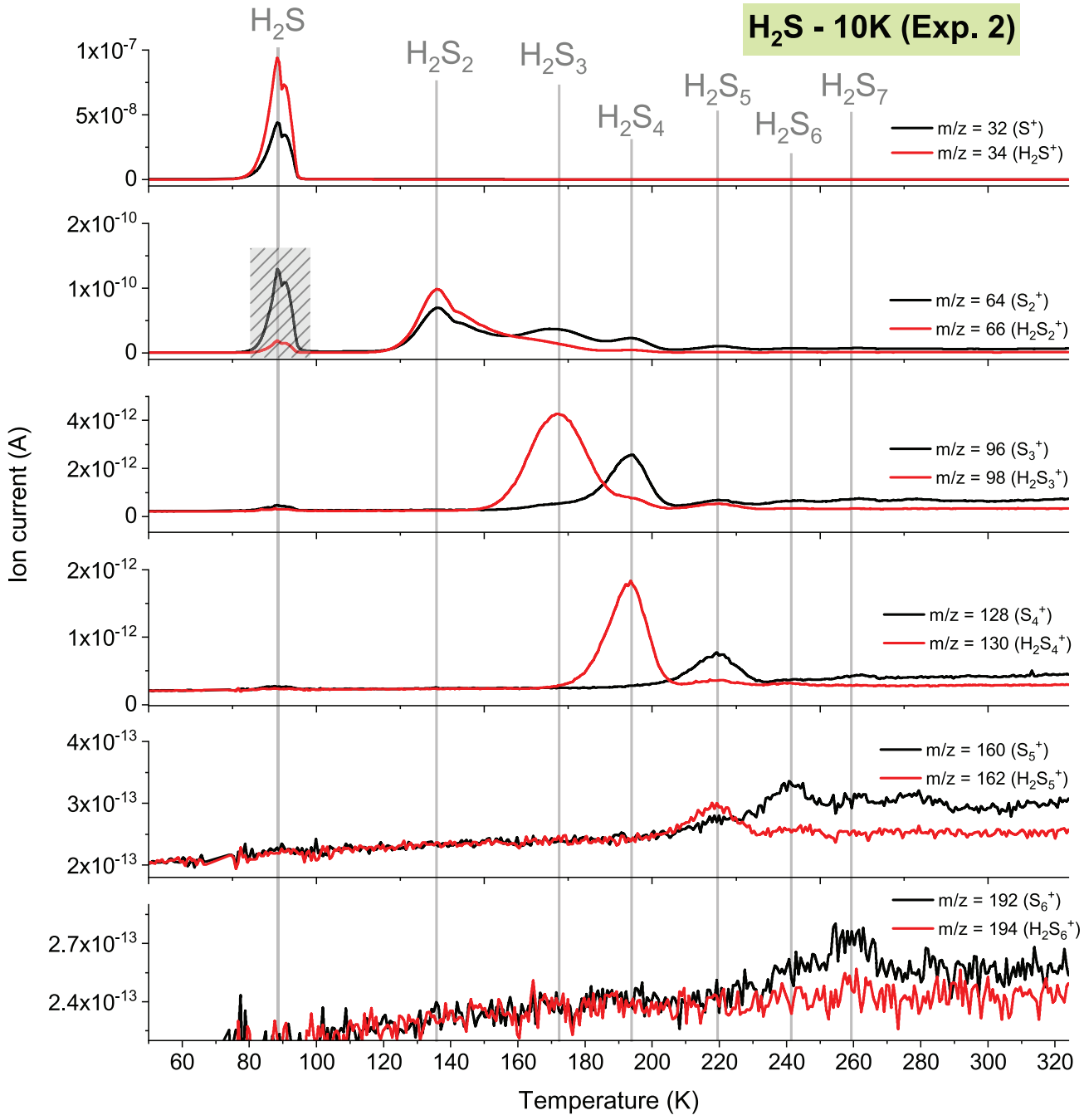

Figure 1. QMS data recorded during thermal desorption of H_2S ice sample deposited and irradiated at 10 K and irradiated at the same temperature (Exp. **2**). $\frac{m}{z}$ fragments related to S_x and H_2S_x, $x = 1$–6 are presented. Vertical lines indicate desorbing species at specific temperatures. Grey area corresponds to contamination coming from deposition, which was also observed in blank experiment, see Section 3.1.

still dominate for larger species. If larger H_2S_x species are formed, the M^+ may not be intense enough to be detectable (as it is the case of H_2S_6 and H_2S_7 in Fig. 1), but $\frac{m}{z} = 64$ may still be observable.

Fig. 3 shows the thermal desorption profile of $\frac{m}{z} = 64$ in Exps **1**, **2**, and **3**. This figure clearly shows desorption peaks at different temperatures, which are coincident with thermal desorption of the H_2S_x species up to H_2S_7. Furthermore, another two thermal desorption peaks are detected, which may be attributed to H_2S_8 and H_2S_9 molecules.

Another piece of evidence supporting the formation of these large polysulphides is related to their thermal desorption temperature. Experimental desorption temperatures confirm that each sulphur atom added to the chain will increase the thermal desorption temperature, but its relative significance in the species will decrease as the chain becomes longer. Therefore, an exponential fit is proposed to adjust thermal desorption temperature of H_2S_x species up to H_2S_5 (blue dashed line in Fig. 4). This exponential fit should then predict thermal desorption temperature for larger species. As shown in Fig. 4, this fit underestimates thermal desorption temperature for H_2S_6 and H_2S_7. Nevertheless, adding experimental desorption temperatures of H_2S_6 and H_2S_7 (orange dotted line), it also results in a good exponential fit.

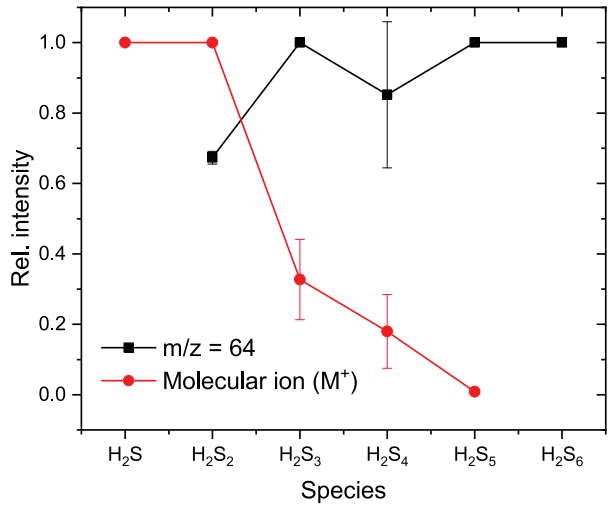

Figure 2. Relative intensity of $\frac{m}{z}$ fragment 64, and molecular ion (M^+) fragment for H_2S_x species up to H_2S_6 in the mass spectra of each species (from Exps **2** and **3**). As the number of S atoms in the molecule becomes larger, molecular ion fragment is less significant, while $\frac{m}{z} = 64$ becomes the most intense feature in the mass spectra (see Fig. 5). Errors were obtained from the standard deviation of Exps **2** and **3**.

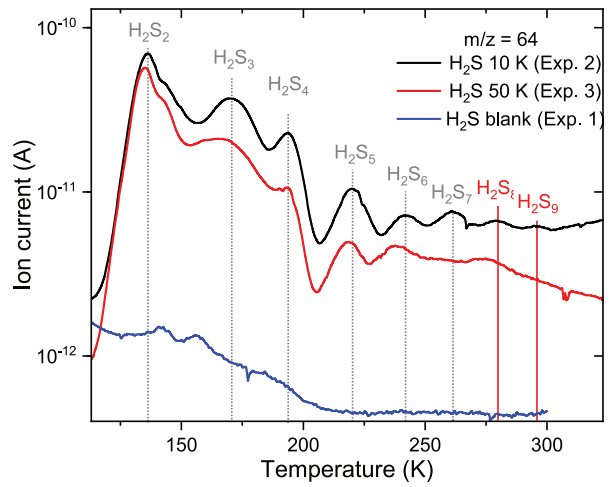

Figure 3. $\frac{m}{z} = 64$ recorded for Exps **1, 2,** and **3** during warm-up of the ice samples. Fig. 5 suggests that $\frac{m}{z} = 64$ is the most intense mass fragment for H_2S_x species when x is large enough. Therefore, the two desorption peaks located at 280 and 296 K could be attributed to thermal desorption of H_2S_8 and H_2S_9.

If H_2S_8 and H_2S_9 species are responsible for the desorption peaks at 280 and 296 K, their thermal desorption temperature should be well predicted by the exponential fit in Fig. 4. As it happened for H_2S_6 and H_2S_7, the exponential fit underestimates the desorption temperature for H_2S_8 and H_2S_9. The repeated underestimation of desorption temperatures suggests that the exponential fit is not reproducing well the experimental data for long polysulphides. Pouillot, Chandler & Eckert (1996) studied the sublimation temperatures for alkanes from $C_{20}H_{42}$ to $C_{35}H_{72}$. They fitted thermal desorption temperatures using a linear fit. Green solid line in Fig. 4 shows a linear fit of the last four experimental points, related to H_2S_5–H_2S_9. Looking at the

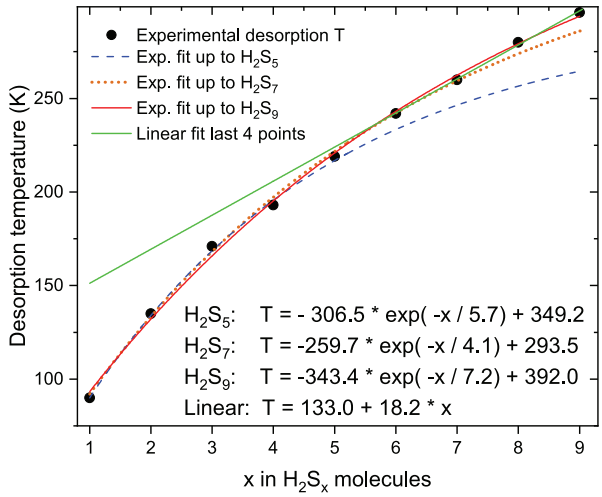

Figure 4. Experimental thermal desorption temperature for H_2S_x species from Exp. **2**. Increasing number of S atoms should increase desorption temperature following an exponential trend (red solid line). Species up to H_2S_9 were detected experimentally.

graph, it seems that the linear fit is adequate when dealing with relatively large species, but it fails for smaller sulphur chains, for which an exponential trend is more consistent with experimental data. Therefore, we consider that this fit would make a better prediction for even longer H_2S_x species.

Fig. 5 and Table 2 present the mass spectra of H_2S_x molecules up to $x = 6$, calculated from laboratory experiments during warming up of photoprocessed pure H_2S ice samples (Exps **2** and **3**). The molecular ion (M^+) is not the most intense peak for those chains containing three or more sulphur atoms. Instead, $\frac{m}{z} = 64$ becomes more intense for longer H_2S_x species. It is important to note that, for all sulphur chains, the $\frac{m}{z} = M$–34 is relatively intense. Looking at the mass spectra at a specific temperature, the detection of M–34 could be wrongly attributed to the presence of the corresponding S_{x-1} molecule, but it would arise from the characteristic fragmentation of H_2S_x.

Table 3 shows the thermal desorption temperature measured for H_2S_x species up to H_2S_9. Last column shows the probability of having one ^{34}S atom in the molecule. As the chains become larger, the fraction of molecules containing the ^{34}S isotope is higher. Therefore, the detection of $\frac{m}{z} = M+2$ is only indicative of the presence of a different species if the expected $\frac{(M+2)}{M}$ ratio is significantly larger than the statistical probability (last column in Table 3). For Exps **2** and **3**, the $\frac{(M+2)}{M}$ ratio was calculated. Results are shown in column 3 of Table 3. Roughly, the isotopic expected ratio was obtained for H_2S_x, $x = 1$–4, meaning that species with H_4S_x as molecular formula are not formed, and the presence of $M+2$ mass fragment is only due to isotopic contribution. For larger polysulphides, the recorded signal of $M+2$ mass-to-charge fragment was not intense enough to calculate the $\frac{(M+2)}{M}$ ratio.

3.2 Water effect on the formation and thermal desorption of sulphur chains

Fig. 6 shows thermal desorption of water molecules in Exps **4** and **5**. Two peaks are observed at 173 and 180 K, probably due to thermal

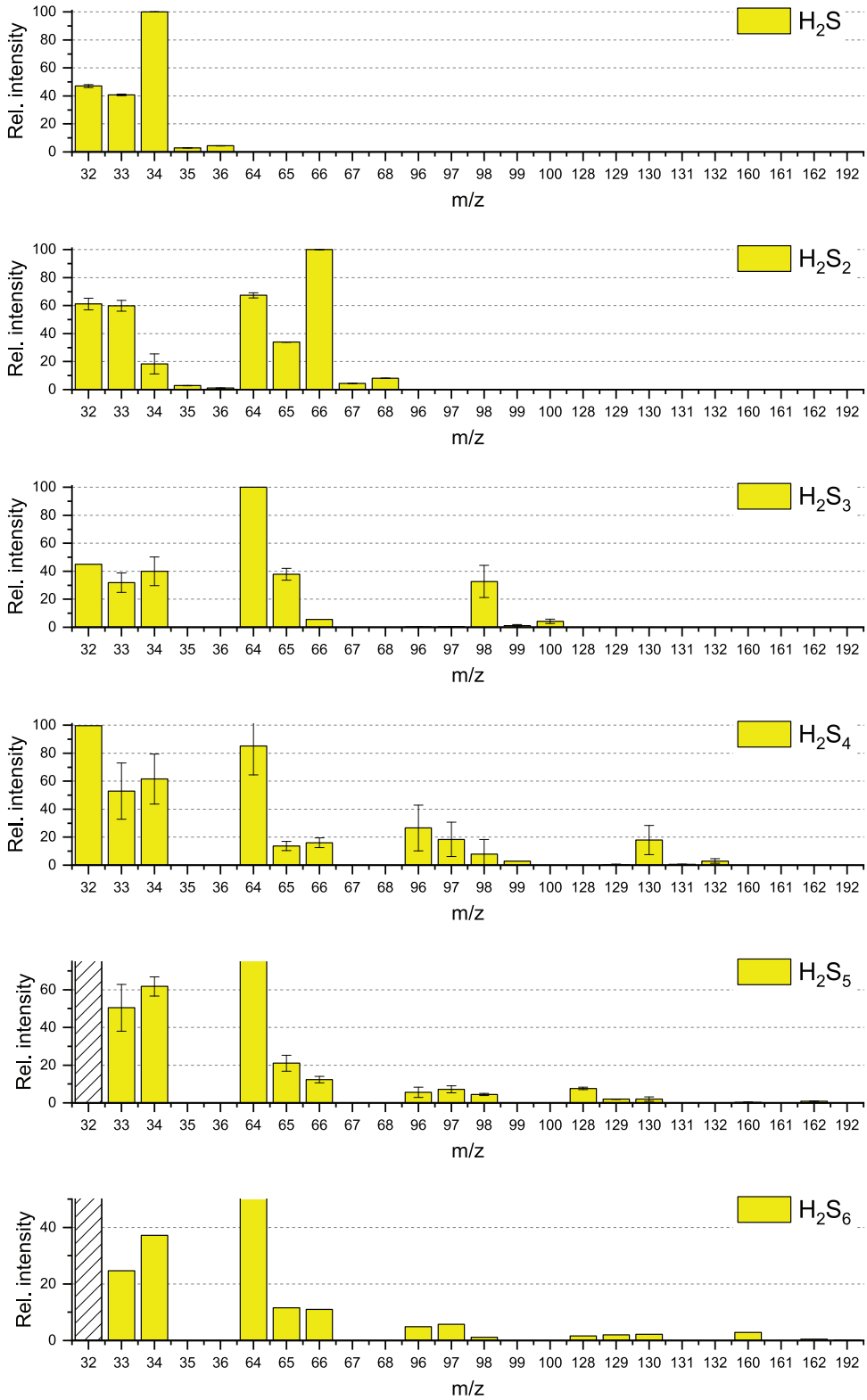

Figure 5. Experimental mass spectra of H_2S_x ($x = 1$–6) molecules obtained during thermal desorption of each species in Exps **2** and **3**. $\frac{m}{z} = 64$ was truncated for H_2S_5 and H_2S_6 to better show the contribution of minor fragments. Intensity of $\frac{m}{z} = 32$ could not be determined for H_2S_5 and H_2S_6 due to the low abundance of these species, and the relatively high baseline of $\frac{m}{z} = 32$. Some error bars are too small to be appreciated in the graph. Error bars for H_2S_6 could not be calculated, as there was not enough signal in Exp. **3** to obtain quantitative results for this species.

Table 2. Mass spectra recorded during thermal desorption of H_2S_x species in Exps **2** and **3** (averaged values). Intensity was normalized to 100 for the most intense $\frac{m}{z}$ ratio of each species.

Species	32	33	34	35	36	64	65	66	67	68	96	97	98	99	100	128	129	130	131	132	160	161	162	192
H_2S	46	40	100	3	4	–	–	–	–	–	–	–	–	–	–	–	–	–	–	–	–	–	–	–
H_2S_2	58	57	13	–	–	69	34	100	4	8	–	–	–	–	–	–	–	–	–	–	–	–	–	–
H_2S_3	45	37	47	–	–	100	35	6	–	–	0.1	0.6	25	0.5	3	–	–	–	–	–	–	–	–	–
H_2S_4	100	39	49	–	–	70	11	14	–	–	15	10	0.3	–	–	–	0.2	10	0.4	2	–	–	–	–
H_2S_5	?	42	58	–	–	100	18	11	–	–	4	6	4	–	–	8	2	1	–	–	0.2	–	0.9	–
H_2S_6	?	25	37	–	–	100	12	11	–	–	5	6	1	–	–	2	2	2	–	–	3	–	0.5	0.2

Table 3. Second column: thermal desorption temperature of H_2S_x species measured in Exps **2** and **3**. Third column: ratio between the ion current measured by the QMS during thermal desorption of H_2S_x species for molecular mass-to-charge ratio (M) and M+2, mostly due to isotopic contribution of ^{34}S atoms. For these ratios, errors are estimated to be about 10 per cent. The low intensity recorded for the corresponding M+2 mass-to-charge in H_2S_x species with $x > 4$ prevented us from calculation of this ratio. Last column shows the probability of ^{34}S in these molecules.

S atoms	T_{des} (K)	Ratio $\frac{(M+2)}{M}$	Probability (per cent)
1	88	4.4	4.2
2	136	8.1	8.3
3	172	13.1	12.2
4	194	16.5	15.9
5	219	–	19.5
6	241	–	22.9
7	259	–	26.2
8	280	–	29.3
9	296	–	32.3

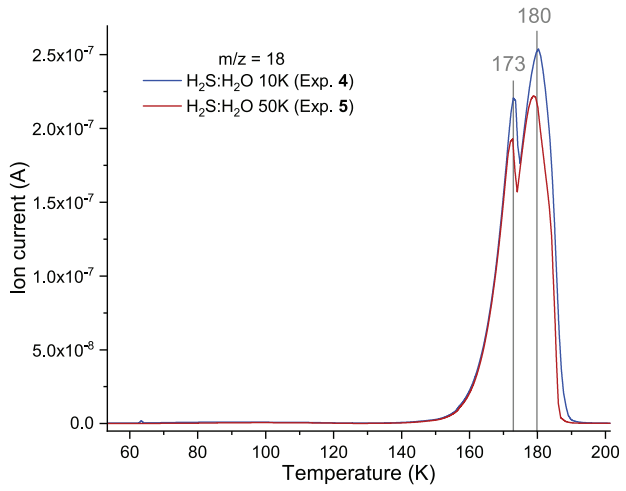

Figure 6. Thermal desorption of water molecules from Exps **4** and **5**. The two desorption peaks could be related to desorption of different crystalline phases of water (i.e. cubic and hexagonal water ice).

desorption of two different water phases. Below 150 K no thermal desorption is observed. Therefore, the thermal desorption observed around 140 K for H_2S_x species in these experiments is not due to co-desorption with water molecules or H_2S (Fig. 7). According to Smith et al. (1997), this desorption is induced by the water transition from amorphous to cubic crystalline structure, ejecting molecules during the process. This effect is known as volcano desorption.

Fig. 7 shows thermal desorption of polysulphides (H_2S to H_2S_7) in H_2O-rich ice samples in Exp. **4**. This figure shows a relatively small thermal desorption of H_2S molecules at the expected temperature from pure H_2S ice (87 K), and a larger volcano desorption during water transition from the amorphous to cubic crystalline structure. As explained in Section 3.1, the $\frac{m}{z} = 64$ signal measured at 88 K is related to contamination, as it happened in Exp. **2**. The larger intensity of $\frac{m}{z} = 64$ recorded during H_2O crystallization could be, in principle, also due to contamination. If this is the case, a similar intensity should be recorded in Exp. **5**. Fig. 8 shows almost no $\frac{m}{z} = 64$ signal at 147 K, negligible in comparison with the signal measured for the 10 K experiment. It can be concluded that S_2 is really formed in the 10 K experiment, but it is not observed in the 50 K experiment. The absence of S atoms and S_2 molecules is indicative of the higher mobility of species at 50 K, determining a larger reactivity of radicals as they are formed, opposite to the accumulative effect described previously for the low temperature experiments. H_2S_x species show a similar behaviour with respect to the 10 K experiment, although some differences regarding their intensity are highlighted hereafter.

Furthermore, the intensity recorded for $\frac{m}{z} = 32$ during thermal desorption of H_2S in Exp. **4** (Fig. 7) is larger than the intensity expected during thermal desorption of H_2S (Fig. 5). Therefore, there is another source of S^+, intense enough to produce such a large difference in the $\frac{m}{z} = 32$ intensity. The source of S^+ could be: (1) fragmentation of S_2 molecules, which seem to be abundant in Exp. **4**, or (2) desorption of S atoms trapped in the water matrix. Our data does not allow us to distinguish both scenarios. However, it can be concluded that during water transition around 148 K, most of the S atoms and S_2 molecules, together with a large fraction of H_2S, would be expelled from the bulk of the ice.

All the H_2S_x species show a small volcano desorption at 148 K during water transition, and a more intense thermal desorption during water desorption at 180 K. Most of the polysulphides are dragged with H_2O molecules during H_2O thermal desorption in Exps **4** and **5**. Interestingly, a relatively small fraction of H_2S_4 and H_2S_5 were detected in the gas-phase (detected by $\frac{m}{z} = 130$ and $\frac{m}{z} = 128$, respectively) at 208 and 222 K, close to their pure thermal desorption temperature (194 and 219 K, Table 3), indicative of a small thermal desorption of the less volatile polysulphides apart from H_2O desorption.

From 260 K, Fig. 7 shows an increase in the intensity of mass-to-charge ratios related to S_x^+ cations. The corresponding H_2S_x mass-to-charge ratios are, however, almost not altered at this temperature, suggesting that non-hydrogenated species are responsible of this effect. On Earth, S_8 is the most stable sulphur allotrope, and previous works have highlighted the efficient formation of S_8 in interstellar ice analogues (Muñoz Caro 2002). According to National Institute of Standards and Technology (NIST) data

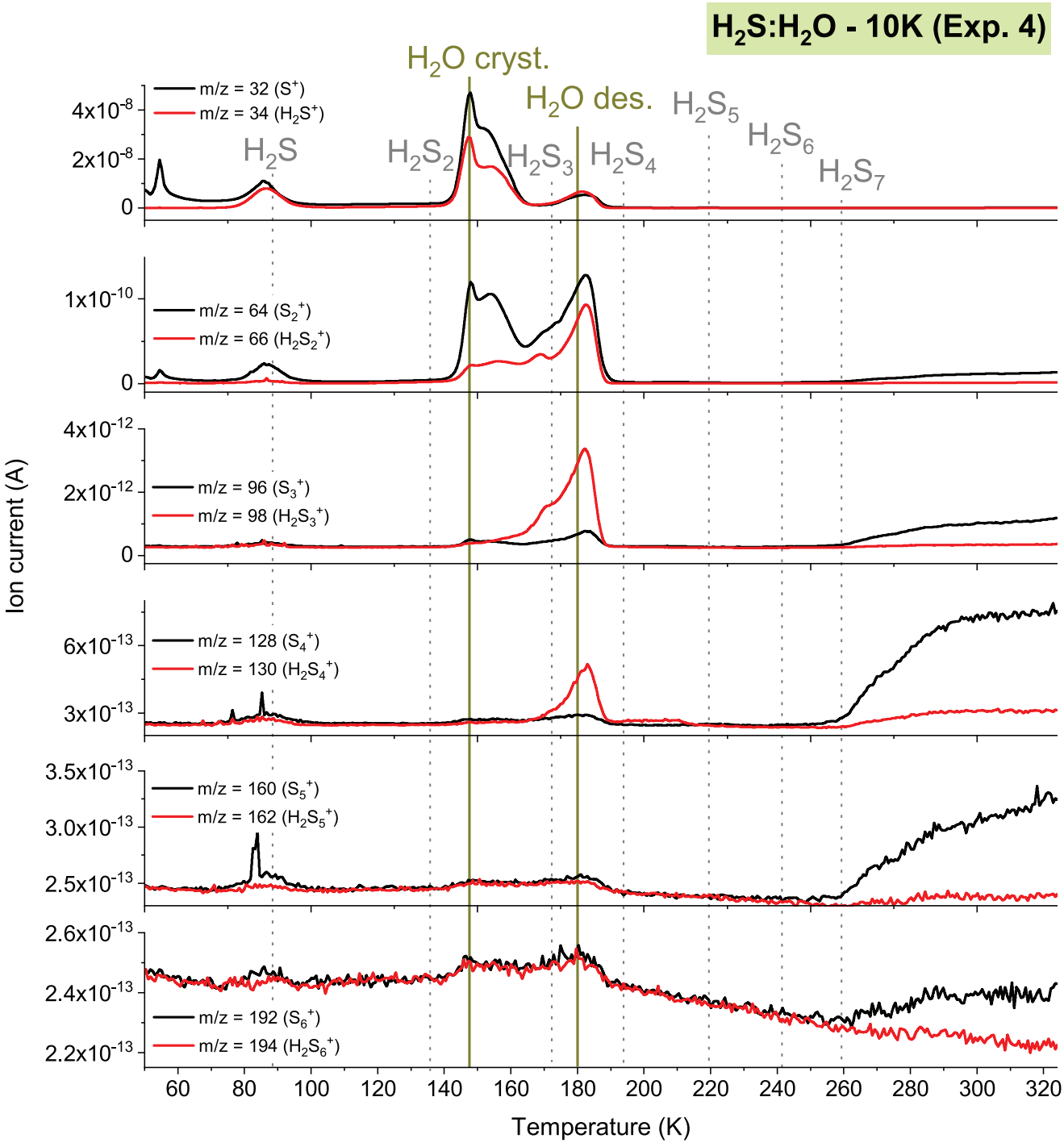

Figure 7. QMS data recorded during TPD of Exp. **4**. $\frac{m}{z}$ fragments related to S_x^+ and $H_2S_x^+$, x = 1–6, ions are shown (same $\frac{m}{z}$ fragments shown in Fig. 1). Vertical dotted lines correspond to thermal desorption of H_2S_x species in Exps **2** and **3**. Vertical brownish green solid lines are related to H_2O crystallization temperature and H_2O thermal desorption. Some sulphur species are ejected from the ice during water transition from amorphous to cubic crystalline ice (volacno desorption, Smith et al. 1997; Martín-Doménech et al. 2014). All sulphur species codesorb in the water ice matrix at 180 K.

base, mass spectra of S_8 produces S_x^+ cations, with x = 2–8. S_7 and S_8 are beyond the limits of our QMS, but the simultaneous increase in the intensity of $\frac{m}{z}$ = 64, 96, 128, 160, and 192 suggest that S_8 could be responsible of this behaviour. Ferreira & Lobo (2011) calculated the low-pressure phase diagram of sulphur, including experimental studies from Bradley (1951) and Briske, Hartshorne & Stranks (1960). The last two works made experiments on the vapour pressure of S_8 as a function of pressure. At the relatively low densities present in the ISM (and reproduced in our chamber), vapour pressure of solid-phase sulphur can induce sublimation from 260 K. A similar effect arises in the 50 K experiment (Fig. 8, Exp. **5**). However, the intensity recorded is much

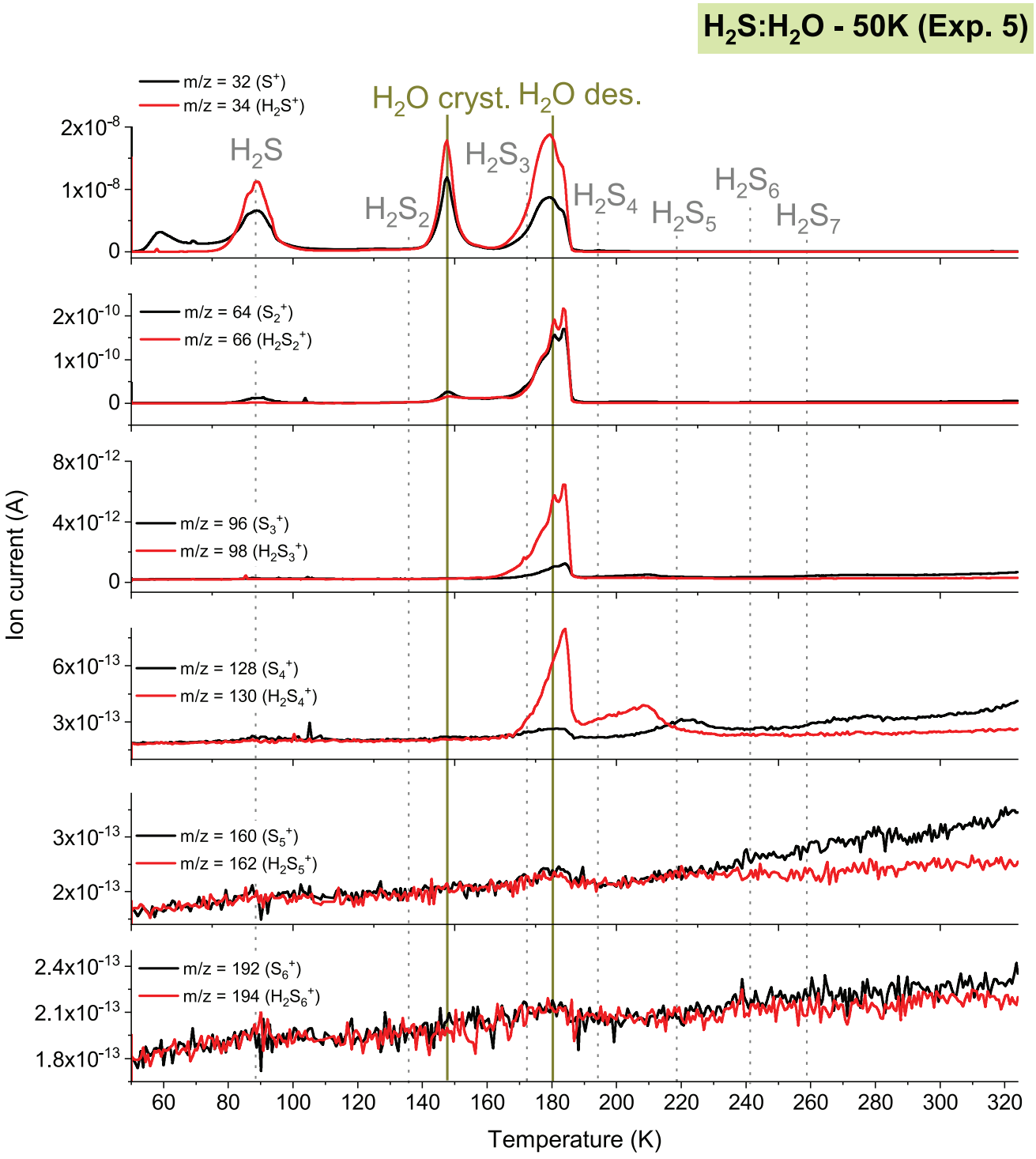

Figure 8. QMS data recorded during TPD of Exp. **5**. $\frac{m}{z}$ fragments related to S_x^+ and $H_2S_x^+$, x = 1–6, ions are shown (same $\frac{m}{z}$ fragments shown in Fig. 1). Vertical dotted lines correspond to thermal desorption of H_2S_x species in Exps **2** and **3**. Vertical dark yellow solid lines are related to H_2O crystallization temperature and H_2O thermal desorption. Desorption of H_2S_x in the lower panels is less intense than the one recorded for Exp. **4** (Fig. 7), indicative of the lower formation of long sulphur chains at 50 K, see the text.

lower, suggesting that S_8 is more efficiently formed in the 10 K experiment.

After UV irradiation of H_2S:H_2O ice mixtures, no S–O bonds are detected in the IR spectrum, meaning that the formation of SO or SO_2 is not as favoured as the formation of sulphur chains, even though water was 4 times more abundant than H_2S molecules. This effect reveals that chemical reactions between sulphur species prevail over sulphur species reacting with water molecules or OH· radicals, as observed by Jiménez-Escobar & Muñoz Caro (2011).

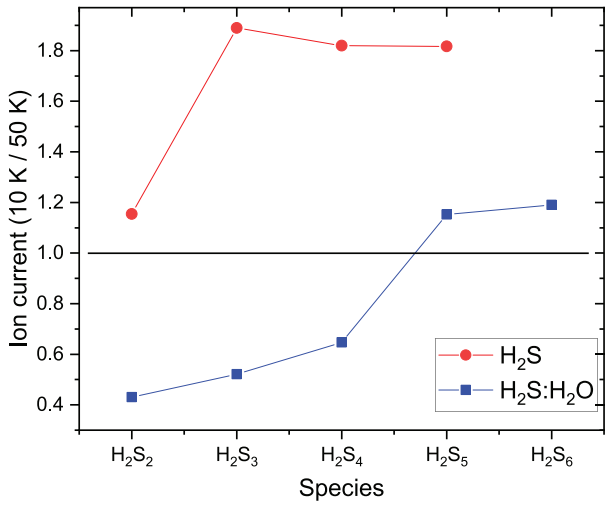

Figure 9. Ratio between the QMS signal recorded for experiments at 10 K (Exps **2** and **4**) and experiments performed at 50 K (Exps **3** and **5**) during thermal desorption of each of the H_2S_x species. While absolute quantification of the abundance of each species requires non-available data from each molecule (see Martín-Doménech et al. 2015), the ratio between the abundance of a given species can be calculated directly from the QMS signal using the molecular fragment, M. Larger H_2S_x species have a molecular mass larger than 200 a.m.u, which is the largest mass-to-charge ratio that can be measured by our QMS.

3.3 Temperature effect

Fig. 9 shows the ratio between the ion current measured for the molecular ion during thermal desorption of H_2S_x in the low temperature and high temperature experiments, both H_2S pure and H_2S:H_2O ice mixtures. A ratio greater than 1 is therefore indicative of the larger formation of a given species in the 10 K experiments. Regarding experiments with pure H_2S ice samples, the formation of H_2S_x species is favoured at 10 K, specially long chains ($x \geq 3$), for which the ion current measured during thermal desorption is almost double of the one measured for the low temperature experiment. On the other hand, H_2S:H_2O ice mixtures showed a larger formation of short sulphur chains ($x \leq 4$) at 50 K, while the formation of long sulphur chains was almost the same at both temperatures.

A likely explanation of this effect is as follows: concerning pure H_2S ice samples, UV photons absorbed by H_2S molecules will mainly produce HS· radicals. At high temperature, as HS· radicals are produced, they will diffuse through the ice and react, forming H_2S_2, or relatively short chains, which are observed in similar abundances at both temperatures. At low temperature, as the mobility of these radicals is reduced and the porosity of the ice is increased, there is an accumulative effect of HS· along irradiation. During warming up of the ice samples, at a specific temperature, pores are expected to coalesce (Cazaux et al. 2015), enabling radicals to diffuse and react, all of them at nearly the same time, favouring the formation of larger chains. As a result, for pure H_2S ice samples, the formation of long sulphur chains is almost doubled at 10 K. Indeed, H_2S_x, $x \geq 7$, were not detected during the high temperature experiment (see Fig. 3). Radicals produced from irradiation of H_2S:H_2O ice mixtures will also be more reactive at 50 K, what determines the higher abundance of short chains at 50 K. The accumulative effect of radicals in the 10 K experiment determines an increase in the 10 K/50 K ratio for the larger polysulphides.

Sulphur detection agrees with previous explanation. S_8 can be formed from successive addition of S atoms, or by dehydrogenation of H_2S_x species. As shorter S_x species were not detected, the first mechanism is less probable. If S_8 is produced from dehydrogenation of H_2S_x, the larger formation of large polysulphides at low temperature will favour the formation of S_8, which is, in fact, more abundant in the 10 K experiment.

4 COMPARISON WITH *ROSETTA*

Experiments suggest that H_2S_x species are formed both in pure H_2S ice and H_2S:H_2O ice mixtures. The detection of these species in the gas-phase is, however, highly dependant on the environment. In water matrix, most of the photoproducts are co-desorbing following H_2O ice crystallization or H_2O thermal desorption. Surrounded by H_2S, each species sublimated at a specific temperature, shown in Table 3.

Calmonte et al. (2016) reported the first detection of several sulphur bearing molecules in comet 67P/Churyumov–Gerasimenko, as measured with the ROSINA mass spectrometer. In particular, they measured a peak related to signal $\frac{m}{z} = 96$, which was attributed to the S_3^+ cation. As the comet got closer to the perihelion, an extended mass range of the mass spectrometer revealed also the presence of $\frac{m}{z} = 128$, which was related to S_4^+ cation. However, as noted by the authors, the lack of experimental data prevented them from confirming the parent molecules of these cations. Figs 1, 5, and Table 2 suggest that H_2S_4 and H_2S_5 may be the parent molecules producing $\frac{m}{z} =$ 96, 128. The molecular mass fragment for these species (mass 130 and 162, respectively) may have an intensity too low to be detected with ROSINA, leaving the *M*–34 fragments as the most characteristic mass-to-charge units, in line with the mass spectra measured in our experiments (see Fig. 5).

As shown in Fig. 1, thermal desorption of polysulphides is, as expected, less abundant as the chain size increases. Therefore, if H_2S_4 and H_2S_5 are the molecules present in the mass spectra of ROSINA presented by Calmonte et al. (2016), H_2S_2 and H_2S_3 might be also detected. Calmonte et al. (2016) reported upper limits for the detection of H_2S_2. However, as stated by the authors, the lack of experimental data for ionization cross-section and fragmentation pattern for H_2S_2 induced a large error on these calculations. They assumed the fragmentation pattern of C_2H_2, which, according to NIST data base and the mass spectra shown in Fig. 5, are significantly different. This fact, combined with the large variety of species which may contribute to $\frac{m}{z} = 66$, may hinder the detection and quantification of H_2S_2. The detection of H_2S_3 with ROSINA was recently reported by Mahjoub et al. (2023), meaning that $\frac{m}{z} =$ 98 was also present in the mass spectra. Larger chains may be present in comet 67P, but an extended mass-to-charge range and better sensitivity might be needed to detect their presence.

However, results presented in Section 3 show another possibility. S_8 molecules may be sublimating from the ice structure. The fragmentation pattern of S_8 is mainly formed by S_x^+, $2 \geq x \leq 8$, cations. The mass range of ROSINA (up to 150 a.m.u) included S_2^+, S_3^+, and S_4^+ mass-to-charge fragments, but longer chains, even if present, would not have been detected. With this work, we propose two possibilities for the identification of the parent molecules in comet 67P: (1) H_2S_4 and H_2S_5 to be responsible of those S_3^+ and S_4^+ cations, respectively, or (2) S_8 species, sublimating and being fragmented in the mass spectrometer. If S_8 is the parent molecule, then S_5^+ and S_6^+ cations could be also detected if the mass spectrometer would have allowed detection at larger a.m.u.

5 CONCLUSIONS AND ASTROPHYSICAL IMPLICATIONS

In this work, we studied experimentally H_2S ice samples, as well as more realistic H_2S:H_2O ice mixtures, regarding the formation of polysulphides and sulphur allotropes. Most important conclusions extracted from this work are highlighted here:

(i) Irradiation of H_2S ice samples led to thermal desorption of H_2S_x species up to H_2S_9. Exponential and linear fits of these temperatures suggest that thermal desorption temperature of larger polysulphides can be predicted using the $T_{des} = 133 + 18.2 \cdot x$ linear fit, for H_2S_x species. Consequently, large polysulphides may be present in the gas-phase of star-forming regions and protoplanetary discs at the given thermal desorption temperatures (Table 3).

(ii) In contrast, H_2O-rich ice samples showed thermal desorption of large polysulphides at two specific temperatures. At 148 K in laboratory experiments (≈98 K in space), a volcano desorption was found, due to H_2O transition from amorphous to cubic crystalline ice. At 180 K in laboratory experiments (≈120 K in space) there is a second desorption during H_2O pure thermal desorption, which drags most of the polysulphides remaining in the ice matrix. Only a small fraction of H_2S_4 and H_2S_5 were detected during thermal desorption at temperatures larger than H_2O desorption. Furthermore, the detection temperature of H_2S_x could be indicative of the pure or mixed composition of the ice mantle.

(iii) H_2S embedded in water molecules is able to form sulphur allotropes, which converge into the final formation of S_8. Although the vapour pressure of S_8 may induce its desorption at the low pressures present in the ISM, it is not expected to have S_8 in the gas-phase. Sulphur sublimation measured from 260 K in our experiments, in contrast with S_8 detection in the solid residue at 300 K (e.g. Muñoz Caro 2002) reveal that S_8 can be kept in the solid phase or sublimate depending on the non-covalent interactions established. Heterogeneity of species tend to retain them in the residue, even if those species would sublimate in its pure form.

(iv) The formation of sulphur chains is temperature dependent. Both in H_2S pure ice and H_2S:H_2O ice mixtures, there is a preferential formation of large polysulphides (H_2S_x) when deposition and irradiation take place at low (10 K) temperatures, while shorter species are favoured in high (50 K) irradiation experiments. This effect is explained by the different diffusion of radicals depending on the temperature (Section 3.3). Sublimating S_8 allotrope (detected in H_2S:H_2O ice mixtures) was also more abundant in the low temperature experiment (Figs 7 and 8).

(v) Calmonte et al. (2016) detected S_3^+ and S_4^+ cations with ROSINA instrument onboard on the *Rosetta* mission. The origin of these fragments could be: (1) S_3 and S_4 molecules themselves or (2) larger species fragmented in the mass spectrometer into S_3^+ and S_4^+ cations. The lack of experimental data and the mass range of ROSINA (from 1 to 150 a.m.u) prevented them from confirming their origin. We propose H_2S_4 and H_2S_5 as possible parent molecules, which is in line with the H_2S_3 detection reported by Mahjoub et al. (2023). S_8 could also be the parent molecule for these fragments, according to its sublimation observed for temperatures larger than 260 K in H_2S:H_2O ice mixtures. However, the heterogeneous nature of ice mantles suggests that S_8 could be kept in the refractory residue in the ISM, due to non-covalent interactions with more polar species.

(vi) In the ISM, sulphur atoms may react in the translucent phase (Cazaux et al. 2022), thus forming sulphur chains, which would probably end up as the most stable S_8 allotrope. According to our results on ice processing, longer chains are favoured when H_2S photoprocessing takes place at low temperatures, while shorter chains would be formed if irradiation takes place at higher temperatures.

(vii) Mass spectra of H_2S_x species up to H_2S_6 have been measured for the first time (Fig. 5). As the number of sulphur atoms is increased, the molecular mass-to-charge fragment intensity is lower, while the intensity of the S_{x-1} mass-to-charge fragment increases, what is relevant for the detection of sulphur-based species in the ISM, hot cores, protoplanetary discs and comets. For future observations of sulphur, observations at mass-to-charge ratios of S_x^+ (32, 64, 96, 128, 160, 192...) and $H_2S_x^+$ cations (34, 66, 98, 130, 162, 194...) will allow to determine whether the observations can be linked to the presence of long sulphur chains, and distinguish whether polysulphides of sulphur allotropes are present by comparing with the mass spectra reported here. A mass range up to 256 a.m.u will be required to detect the presence of S_8.

ACKNOWLEDGEMENTS

This research was funded by project PID2020-118974GB-C21 by the Spanish Ministry of Science and Innovation. The project leading to these results has received funding from 'La Caixa' Foundation, under agreement LCF/BQ/PI22/11910030. This project is co-funded by the European Union (ERC) under ERC-AdG-2022 grant SUL4LIFE (GA 101096293).

DATA AVAILABILITY

The data underlying this article are available in the article.

REFERENCES

Altwegg K. et al., 2022, MNRAS, 516, 3900
Bradley R.-S., 1951, Proc Roy. Soc. Lond. Ser. A. Math. Phys. Sci., 205, 553
Briske C., Hartshorne N. H., Stranks D. R., 1960, J. Chem. Soc., 1960, 1200
Bulut N. et al., 2021, A&A, 646, A5
Calmonte U. et al., 2016, MNRAS, 462, S253
Caselli P., Hasegawa T. I., Herbst E., 1994, ApJ, 421, 206
Cazaux S., Bossa J. B., Linnartz H., Tielens A. G. G. M., 2015, A&A, 573, A16
Cazaux S., Carrascosa H., Caro G. M., Caselli P., Fuente A., Navarro-Almaida D., Riviére-Marichalar P., 2022, A&A, 657, A100
Chen Y.-J., Chuang K.-J., Muñoz-Caro G. M., Nuevo M., Chu C.-C., Yih T.-S., Ip W.-H., Wu C.-Y. R., 2014, ApJ, 781, 15
Collings M. P., Anderson M. A., Chen R., Dever J. W., Viti S., Williams D. A., McCoustra M. R. S., 2004, MNRAS, 354, 1133
Cruz-Diaz G. A., Muñoz Caro G. M., Chen Y. J., Yih T. S., 2014, A&A, 562, A119
Duley W., Millar T., Williams D., 1980, MNRAS, 192, 945
Ferreira A., Lobo L., 2011, J. Chem. Therm., 43, 95
Goesmann F. et al., 2015, Science, 349, 2.689
González Díaz C., Carrascosa H., Muñoz Caro G. M., Satorre M. A., Chen Y.-J., 2022, MNRAS, 517, 5744
Jenkins E. B., 2009, ApJ, 700, 1299
Jiménez-Escobar A., Muñoz Caro G. M., 2011, A&A, 536, A91
Kharma A., Grman M., Misak A., Domínguez-Álvarez E., Nasim M. J., Ondrias K., Chovanec M., Jacob C., 2019, Molecules, 24, 1359
Laas J. C., Caselli P., 2019, A&A, 624, A108
Mahjoub A. et al., 2023, Sci. Adv., 9, eadh0394
Martín-Doménech R., Manzano-Santamaría J., Muñoz Caro G. M., Cruz-Díaz G. A., Chen Y. J., Herrero V. J., Tanarro I., 2015, A&A, 584, A14

Martín-Doménech R., Muñoz Caro G. M., Bueno J., Goesmann F., 2014, A&A, 564, A8
Mastrapa R., Sandford S., Roush T., Cruikshank D., Dalle Ore C., 2009, ApJ, 701, 1347
Muñoz Caro G. M., 2002, PhD. thesis
Muñoz Caro G. M., Jiménez-Escobar A., Martín-Gago J. Á., Rogero C., Atienza C., Puertas S., Sobrado J. M., Torres-Redondo J., 2010, A&A, 522, A108
Oppenheimer M., Dalgarno A., 1974, ApJ, 187, 231
Penzias A. A., Solomon P. M., Wilson R. W., Jefferts K. B., 1971, ApJ, 168, L53
Pouillot F. L. L., Chandler K., Eckert C. A., 1996, Ind. Eng. Chem. Res., 35, 2408
Ruffle D. P., Hartquist T. W., Caselli P., Williams D. A., 1999, MNRAS, 306, 691
Shingledecker C. N., Lamberts T., Laas J. C., Vasyunin A., Herbst E., Kästner J., Caselli P., 2020, ApJ, 888, 52
Smith R. S., Huang C., Wong E., Kay B. D., 1997, Phys. Rev. Lett., 79, 909
Yarnall Y. Y., Hudson R. L., 2022, ApJ, 931, L4

This paper has been typeset from a TEX/LATEX file prepared by the author.